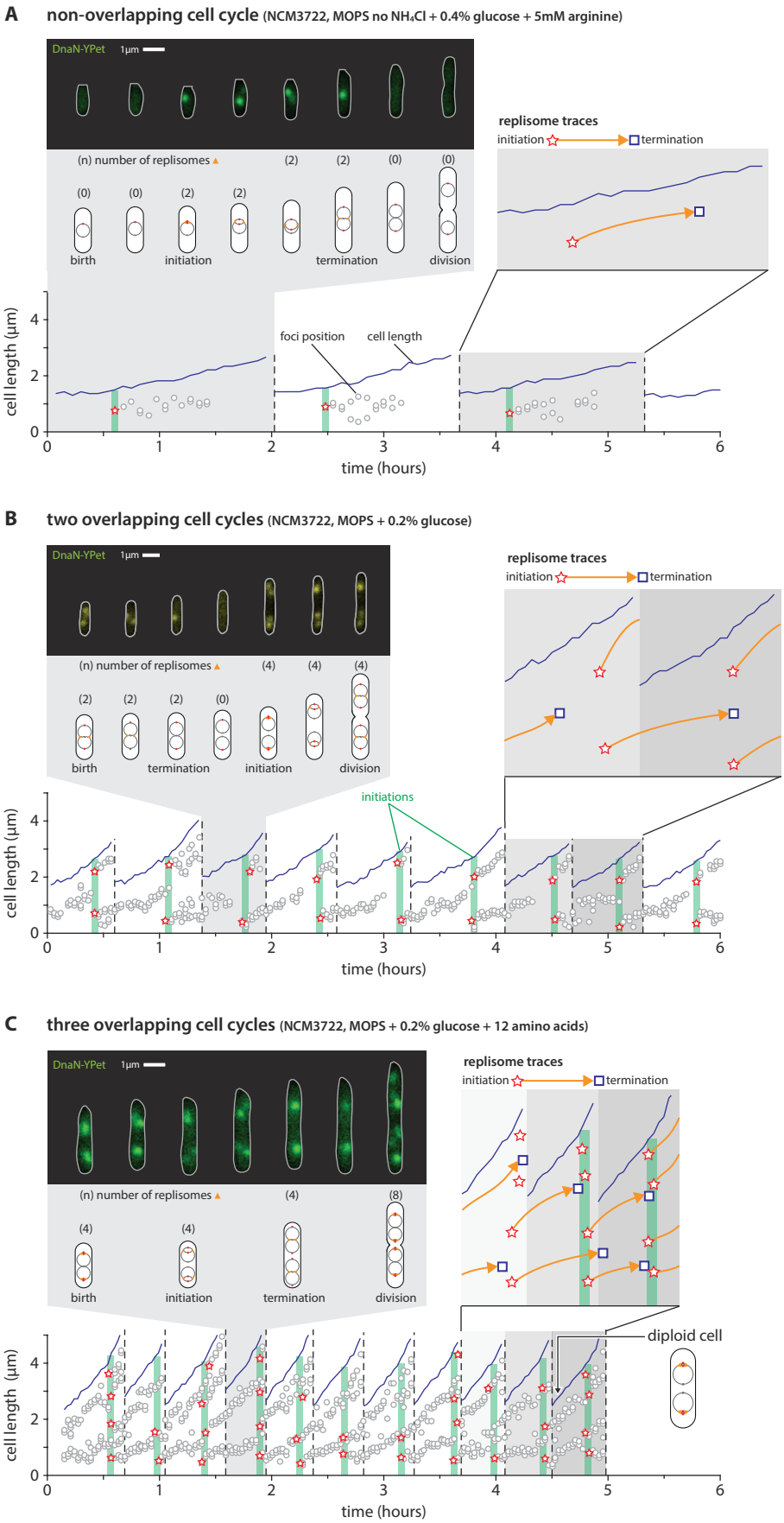
A non-overlapping cell cycle (NCM3722, MOPS no NH4Cl + 0.4% glucose + 5mM arginine)
DnaN-YPet 1µm
(n) number of replisomes
(0) (0) (2) (2) (2) (2) (0) (0)
birth
initiation
termination
division
replisome traces
initiation
termination
foci position
cell length
cell length (µm)
time (hours)
B two overlapping cell cycles (NCM3722, MOPS + 0.2% glucose)
DnaN-YPet 1µm
(n) number of replisomes
(2) (2) (2) (0) (4) (4) (4)
birth
termination
initiation
division
replisome traces
initiation
termination
initiations
cell length (µm)
time (hours)
C three overlapping cell cycles (NCM3722, MOPS + 0.2% glucose + 12 amino acids)
DnaN-YPet 1µm
(n) number of replisomes
(4) (4) (4) (8)
birth
initiation
termination
division
replisome traces
initiation
termination
diploid cell
cell length (µm)
time (hours)

Figure S1: Visualizing and quantifying cell cycle in single bacterial cells in different growth conditions. Related to Figure 1.
We measured cell cycle and cell size simultaneously for many consecutive cell division cycles using microfluidic mother machine in different growth conditions. Here **(A)**-**(C)** show the results of three nutrient conditions where the cells are growing with non-, two and three overlapping cell cycles, respectively. The cartoons show the configuration of chromosome replication in one division cycle, similar to that in Figure 1. The foci positions along the long axis of the cell clearly display the trace of replisomes, making it possible for high-throughput analysis using custom software (see details of image analysis in STAR Methods; see the full data in Data S1). Note that, in fast growth conditions such as **(C)**, the termination of replication often finishes before the cell birth, and the daughter cells are born as diploid.

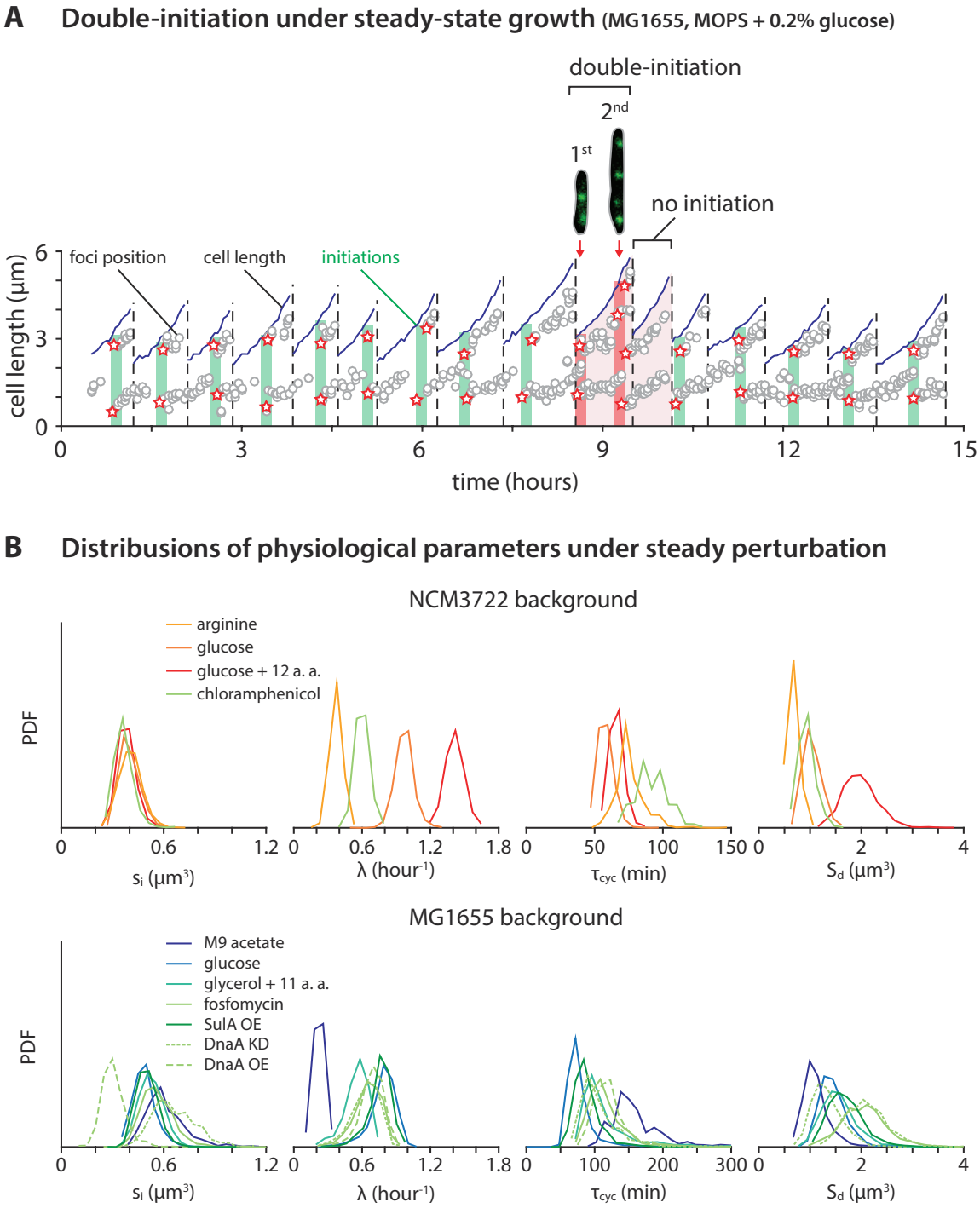

Figure S2: Double-initiation events during steady-state growth due to stochastic cell physiology, and change in major physiological parameters during steady inhibition experiments. Related to Figures 1 and 2.

(A) The decoupling between replication initiation and cell division is evident even from our results of steady-state growth. In the growth condition shown in the figure, cells mostly are with two-overlapping cell cycle, namely, origins duplicate from 2 to 4 at initiation. However, during some division cell cycles, cells fire two rounds of initiations before division, resulting in cells in the next division cycle undergo no initiation. This result disputes the hypothesis that a cell always ensures one-to-one initiation-division correspondence for every division cycle. **(B)** The distributions of major physiological parameters measured from all steady-state experiments as shown in Figure 1D. For a particular strain background, the initiation size per *ori* largely remains the same, despite the changes in growth rate, cell cycle duration (τ_{cyc}) or division size. These single-cell results confirm the invariance of initiation mass observed in previous population-level study [S1].

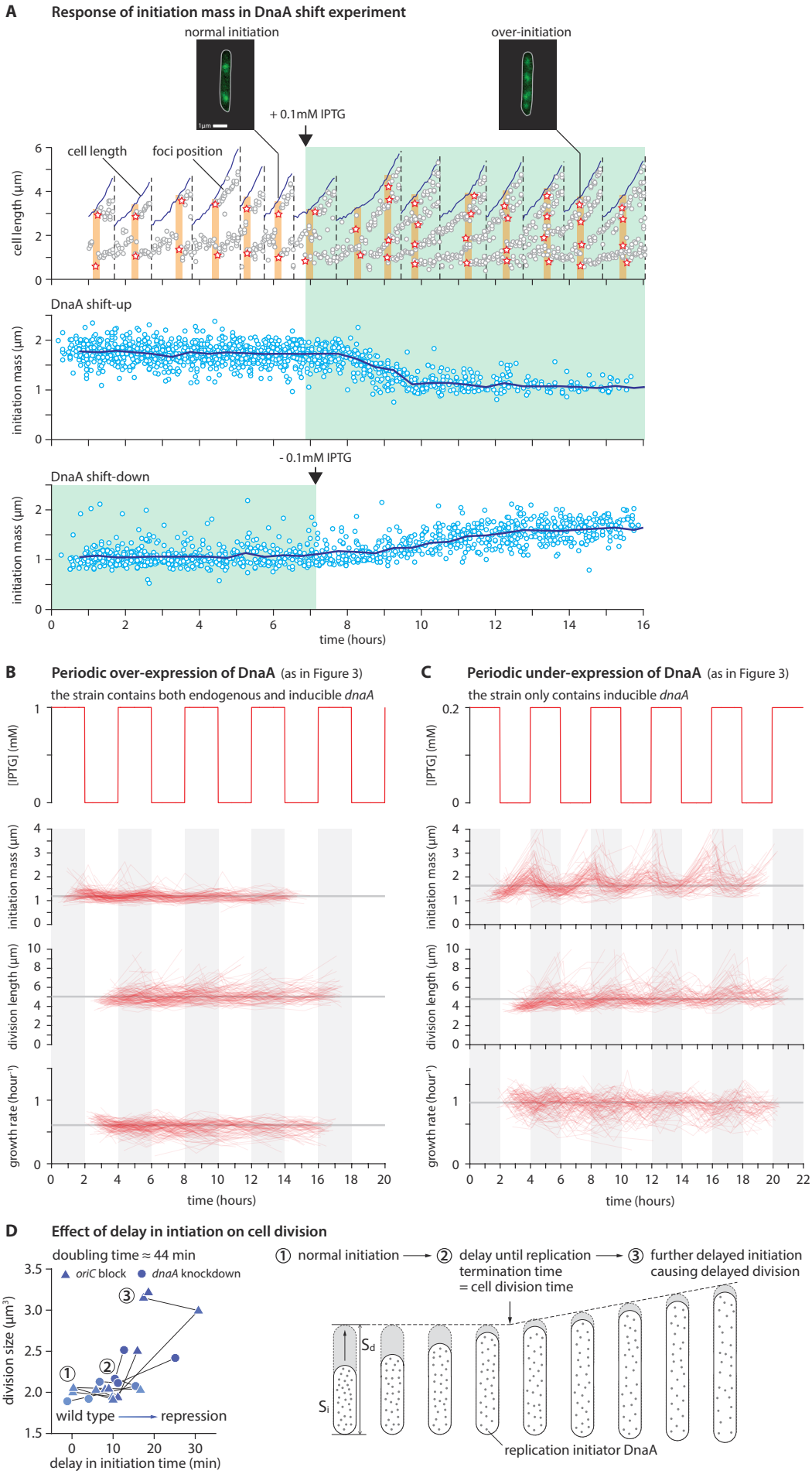
A
Response of initiation mass in DnaA shift experiment
normal initiation
over-initiation
+ 0.1mM IPTG
cell length
foci position
cell length (μm)
DnaA shift-up
initiation mass (μm)
- 0.1mM IPTG
DnaA shift-down
initiation mass (μm)
time (hours)
B
Periodic over-expression of DnaA (as in Figure 3)
the strain contains both endogenous and inducible dnaA
[IPTG] (mM)
initiation mass (μm)
division length (μm)
growth rate (hour⁻¹)
time (hours)
C
Periodic under-expression of DnaA (as in Figure 3)
the strain only contains inducible dnaA
[IPTG] (mM)
initiation mass (μm)
division length (μm)
growth rate (hour⁻¹)
time (hours)
D
Effect of delay in intiation on cell division
doubling time ≈ 44 min
oriC block
dnaA knockdown
division size (μm³)
wild type
repression
delay in initiation time (min)
① normal initiation
② delay until replication termination time = cell division time
③ further delayed initiation causing delayed division
Sd
Si
replication initiator DnaA

Figure S3: Dependency of initiation mass on DnaA level in the DnaA overexpression experiment, and the full data of dynamic perturbation to DnaA expression. Related to Figure 3.

(A) Using a strain carrying extra *dnaA* under P_{lac} promoter on plasmids (see strain information in STAR Methods and Table S1), we induced the overexpression of DnaA by using 0.1mM IPTG and measured the single-cell cell cycle. In this growth condition (MOPS + 0.4% glycerol + 11 aminos acids), cells over-initiated after induction (DnaA shift-up); the origins duplicated from 2 to 4 before induction and 4 to 8 afterwards. Thus our results show that the initiation mass is dependent on DnaA induction level. The reverse process was observed when 0.1mM IPTG was removed (DnaA shift-down). The response time of both shift-up and shift-down took more than one doubling times (average doubling time $\approx$ 61min). Blue lines represent the binned average. **(B)** and **(C)** Grey lines indicate the time averages. Each thin trace connects the values of each generation from a single lineage, same for Figure S**4**. During the oscillation of DnaA induction, initiation mass changed periodically while growth rate and division size were mostly constant. **(D)** The independent control of initiation and division is seen from our previous population-level data [S1]. Using the tunable CRISPR interference system, we delayed the initiation time in a gradual manner. The initiation was delayed by either repressing *dnaA* or blocking *oriC*. When initiation is delayed, the division size remains mostly constant as long as replication termination timing does not exceed the division timing. Thereafter, initiation delay causes an increase in division size.

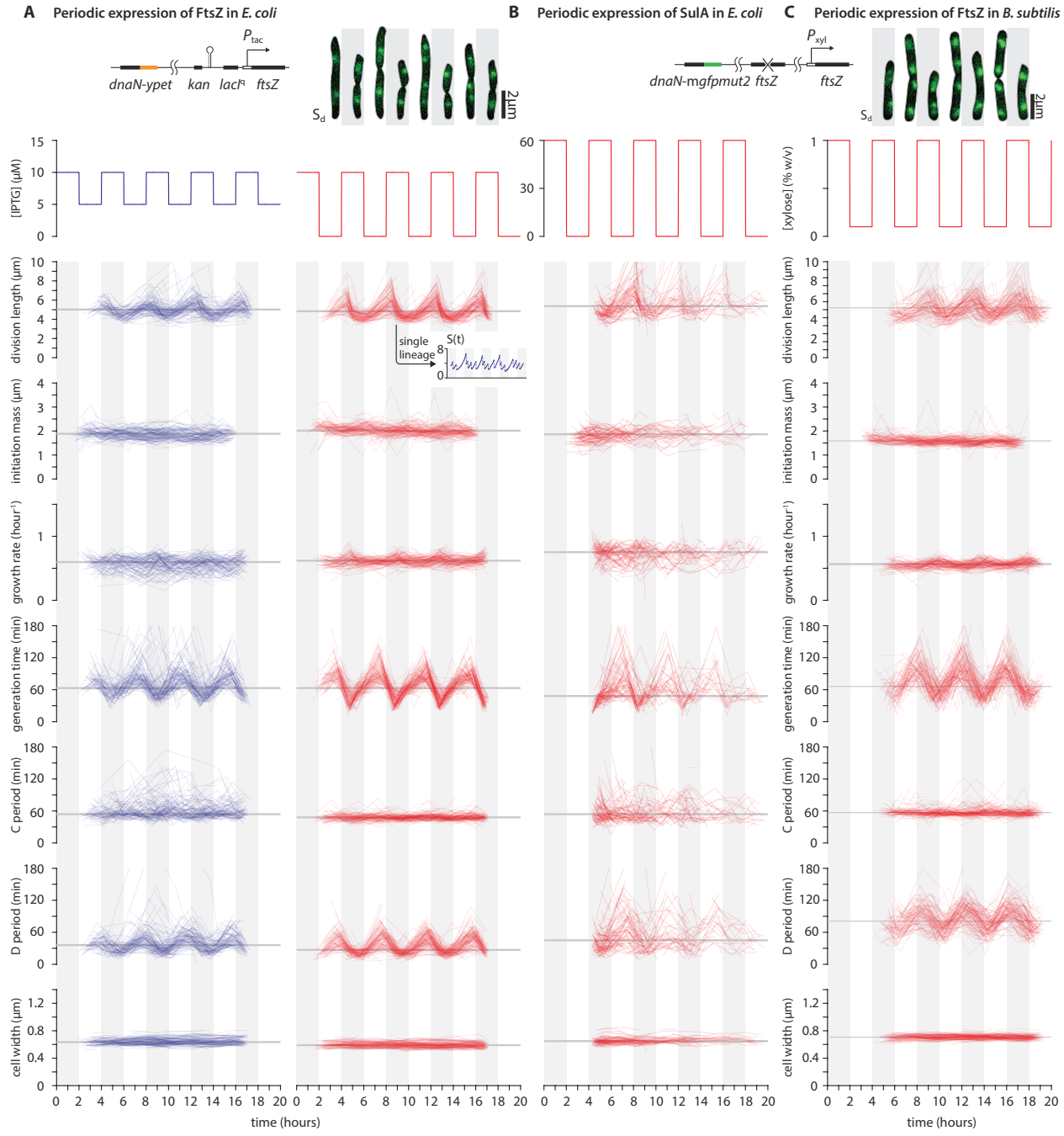
A
Periodic expression of FtsZ in E. coli
B
Periodic expression of SulA in E. coli
C
Periodic expression of FtsZ in B. subtilis
dnaN-ypet kan lacI^q ftsZ
dnaN-mgfpmut2 ftsZ
ftsZ
2μm
[IPTG] (μM)
[xylose] (% w/v)
single lineage
S(t)
division length (μm)
initiation mass (μm)
growth rate (hour⁻¹)
generation time (min)
C period (min)
D period (min)
cell width (μm)
time (hours)

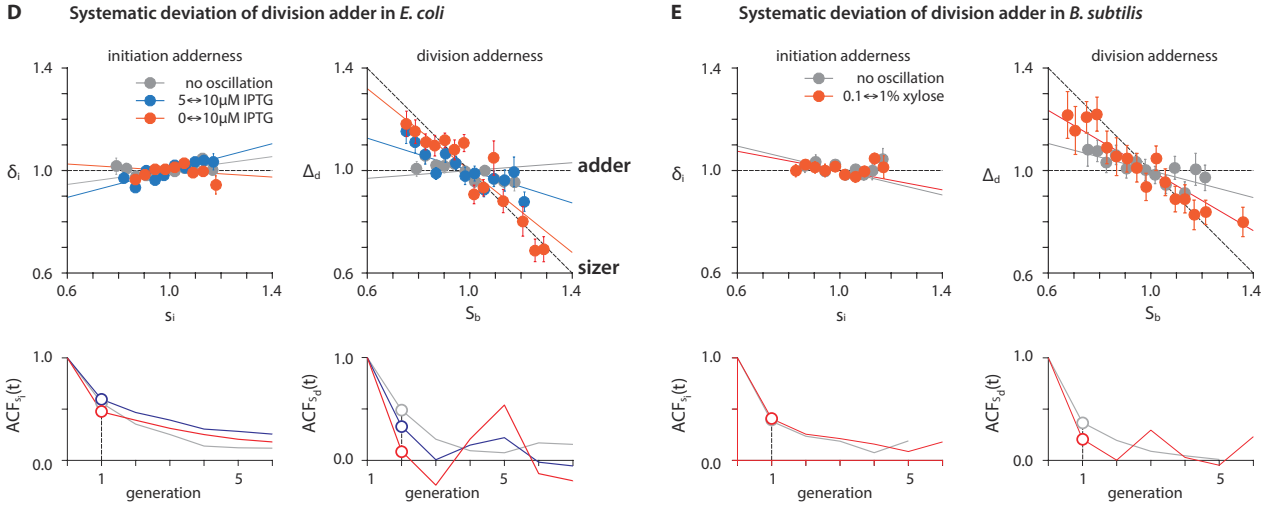
D
Systematic deviation of division adder in E. coli
E
Systematic deviation of division adder in B. subtilis
initiation adderness
division adderness
no oscillation
5↔10μM IPTG
0↔10μM IPTG
0.1↔1% xylose
adder
sizer
generation

Figure S4: Full data of dynamic perturbation to FtsZ expression in *E. coli* and *B. subtilis*. Related to Figure 4.
(A) Top left: The schematics of genetic modifications for the inducible system of division protein and fluorescence replisome markers. In *E. coli*, the native promoter of ftsZ was replaced with a P_{tac} promoter. Top right: The cell images show oscillations of division size in *E. coli* from a single cell lineage (replisome markers overlaid). Bottom: When FtsZ level was oscillated, division size, generation time and D period were oscillating accordingly. In contrast, growth rate and initiation mass were mostly unchanged. The inset in the right column shows how the division size oscillated seen from a single lineage. **(B)** The periodic expression of SulA in *E. coli* has similar effect on the physiological parameters to that of FtsZ. **(C)** Top: In *B. subtilis*, the endogenous ftsZ was deleted while an alternative copy ftsZ under P_{xyl} was inserted at a different loci of the chromosome. The cell images show oscillations of division size in *B. subtilis* from a single cell lineage (replisome markers overlaid). Bottom: When FtsZ level was oscillated, division size, generation time and D period were oscillating accordingly. In contrast, growth rate and initiation mass were mostly unchanged. **(D)** and **(E)** Reprogramming size homeostasis by dynamic modulation of FtsZ in *E. coli* and *B. subtilis* at the oscillation period 4τ. IPTG concentrations: blue = 5 μM -10 μM, red = 0 μM -10 μM. Xylose concentration: blue = 0.1% w/v -1 % w/v. In the correlation plots, the variables are normalized by their means and solid lines are model predictions from Methods S1 I.E.

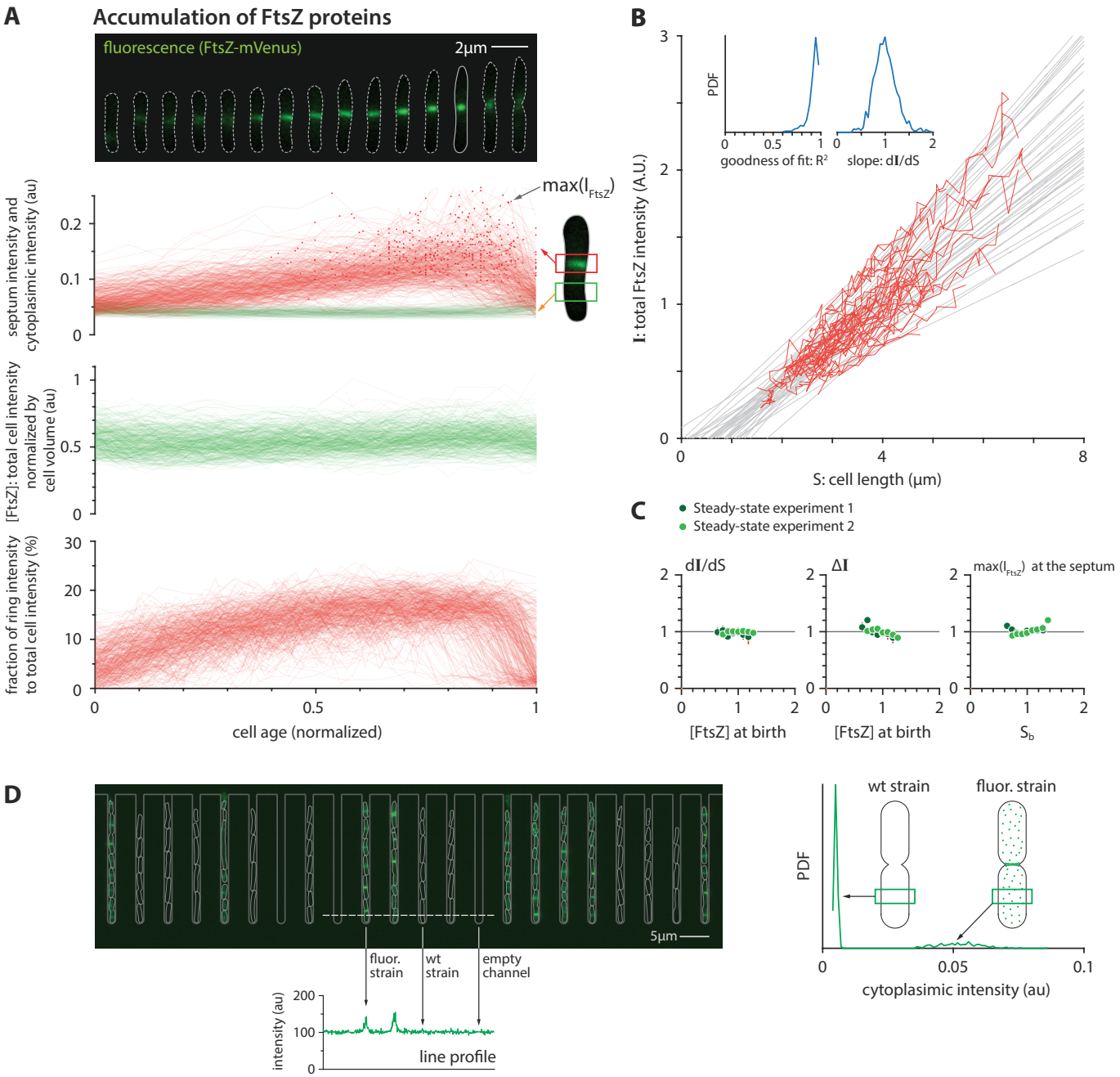

Figure S5: Quantification of FtsZ-mVenus in *E. coli* under steady-state growth. Related to Figure 5.
(A) Steady accumulation of FtsZ at the Z ring "scaffold." The amount of FtsZ accumulated in the ring was estimated by integrating the total fluorescence intensity within a fixed area enclosing the mid-cell region (septum intensity). The cytoplasmic intensity was measured similarly at the first and third quarter positions. The dark red dot on each trace indicates the max total fluorescence in the Z ring, namely, the peak value of the accumulation trace. The ratio of ring intensity to total cell intensity was calculated as the septum intensity subtracting the cytoplasmic intensity divided by the total fluorescence per cell. This ratio approached a nearly constant value in the first half of the division cycle. During this period, the amount of FtsZ at septum well mirrors the total amount in the cell. **(B)** Single-cell growth traces showing that the total FtsZ intensity per cell is linearly proportional to cell volume. The slope of the linear fit was used to estimate dI/dS for each single cell. **(C)** Both the production per volume growth estimated by dI/dS and the threshold estimated by ΔI are largely independent of FtsZ concentration at birth. The max total fluorescence in the Z ring is independent of birth size. In the correlation plots, the variables are normalized by their means. **(D)** The autofluorescence of cytoplasm is negligible compared to the fluorescence of cytoplasmic FtsZ-mVenus. Left: To show this, the strain with FtsZ mVenus (SJ1725) and the parental wild type MG1655 strain (SJ81) were co-grown in mother machine. The cytoplasmic autofluorescence of wild type cells is almost same as that from the empty channels. Right: The mean value of cytoplasmic intensity of wild type cell (n=468) is about 9.5% of that of FtsZ-mVenus cells.

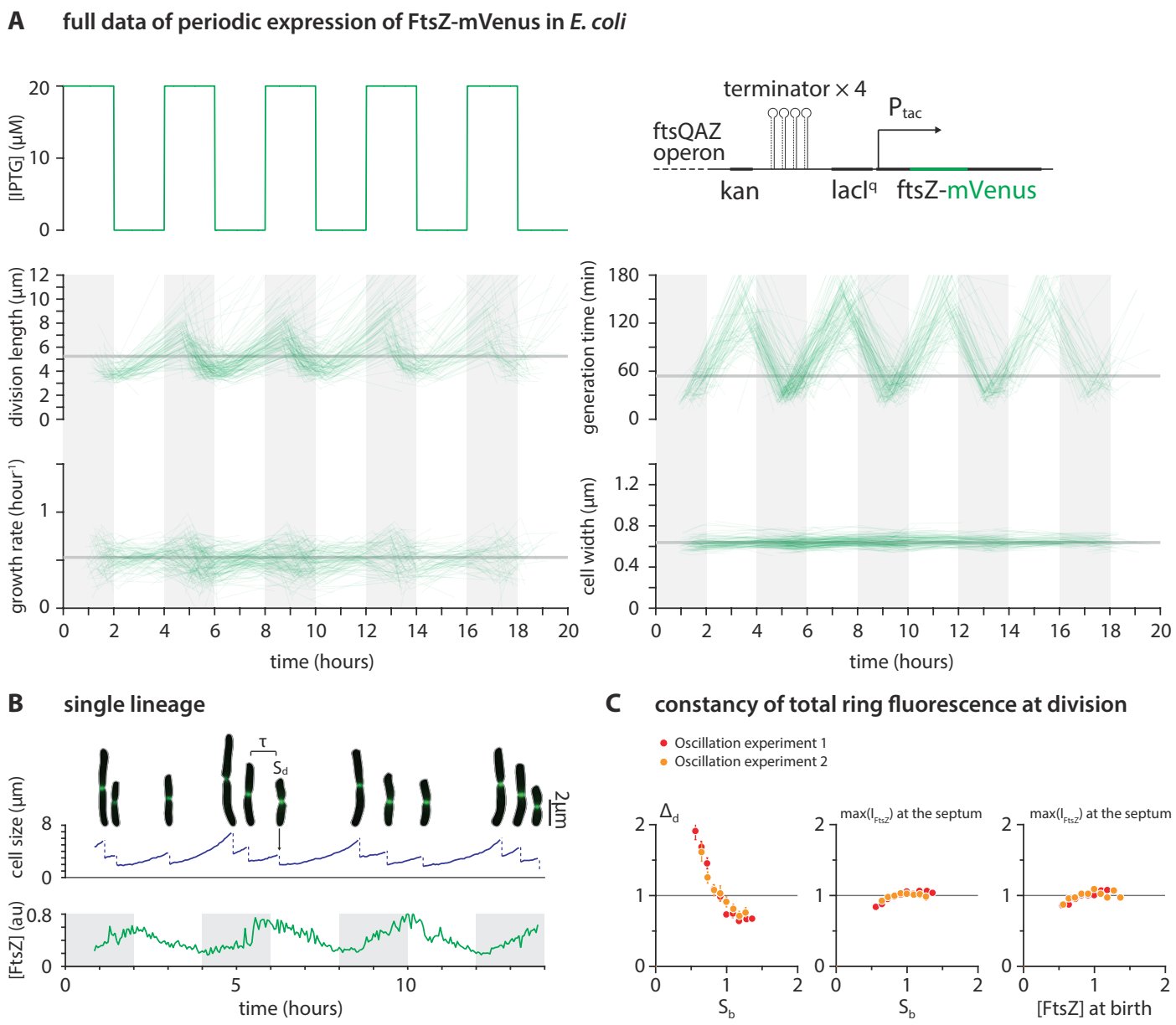

Figure S6: Full data of periodic expression of FtsZ-mVenus in *E. coli*. Related to Figure 6.
(A) When FtsZ level was oscillated, division size and generation time were oscillating accordingly. In contrast, the growth rate showed very mild change. The illustration at top right shows the design of inducible system for *ftsZ* (see strain information in STAR Methods and Table S1). **(B)** The oscillation of division size and FtsZ concentration can be seen from a continuous single lineage. **(C)** The maximal total fluorescence of Z-ring is largely independent of FtsZ concentration and cell size at birth. In the correlation plots, the variables are normalized by their means.

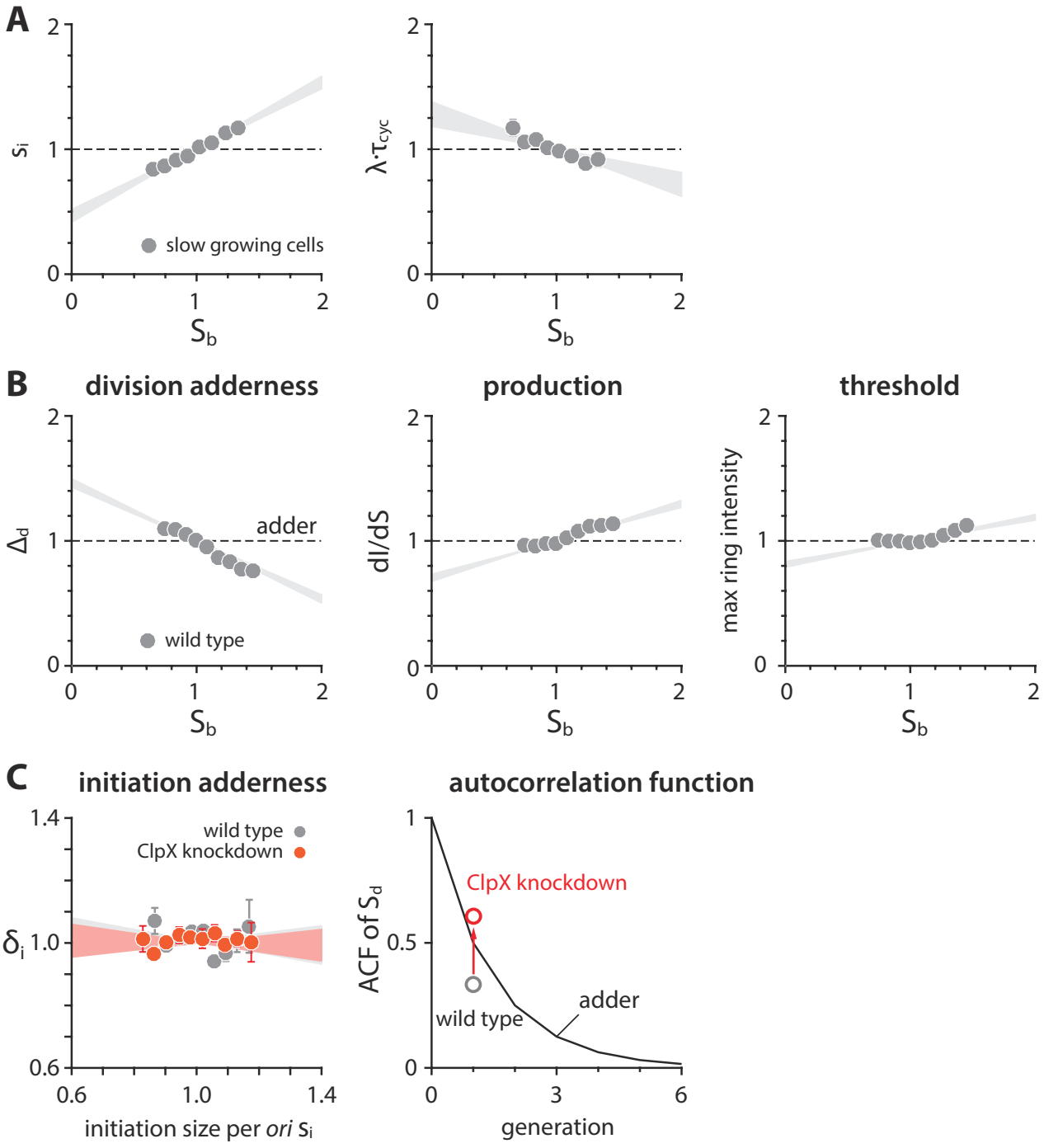

Figure S7: Cell-size homeostasis and production of FtsZ-mVenus in slow growth conditions. Related to Figure 7.
(A) Both s_i and $\lambda \cdot \tau_{cyc}$ show correlation with birth size. **(B)** In slow growth condition, the cell-size homeostasis deviates from adder and the production per volume growth dI/dS is also no longer independent of birth size. In the correlation plots, the variables are normalized by their means. **(C)** In slow-growing *E. coli* cells, repressing *clpX* expression via tCRISPRi restored the division adder, while initiation adder was invariant. Each shaded area represents the 95% confidence interval of linear fit to the respective raw scatter plot.

E. coli strains	Genotype	Experiments used	Notes
SJ358	K-12 NCM3722 F-,	–	background strain; [S2, S3]
SJ81	K-12 MG1655 F- λ- rph-1	–	background strain; low motility [S1]
SJ_XTL219	MG1655 *lacY* A177C, *spec*<>*araFGH*, Δ*lacI* Δ*araE*, P_{BAD}-dCas9, *galM*<pBBa-J23119 *tet-sacB*-handle-(*S. pyogenes* terminator-(*rrnB* terminator)>*gmpA* pSIM18)	–	[S4]
SJ_XTL226	SJ_XTL219 *dnaA* sgRNA, *dnaA*	–	[S1]
VIP205	K-12 MC1061 with native *ftsZ* gene replaced by pTAC-*ftsZ*	–	[S5]
SJ_FS103	SJ358 transduction of *kan-yPet-dnaN*	nutrient limitation (NCM3722), chloramphenicol in Figure 1D	[S6]
SJ_FS104	SJ81 transduction of *kan-yPet-dnaN*	nutrient limitation (MG1655), fosfomycin in Figure 1D; no oscillation data in Figures 2B and 3C	[S6]
SJ_FS105	SJ_XTL226 transduction of *kan-yPet-dnaN*	DnaA knockdown in Figure 1D	This study
SJ_FS110	SJ_FS104 transformation of pDB192 for SulA overexpression	SulA overexpression in Figure 1D	[S7]; This study
SJ_DL91	SJ_FS104 transformation of pSN306 for DnaA overexpression	DnaA overexpression in Figure 1D; DnaA oscillation in Figure 3A	[S8]; This study
SJ_FS112	SJ_FS104 transformation of pLR40 for DnaA overexpression	DnaA overexpression in Figure 1D; Exp. 1 of DnaA oscillation in Figure 3A	[S9]; This study
SJ1436	SJ_FS112 recombineering of ΔdnaA::[P_{cat}::cat<>*dnaA*]	Exp. 2 of DnaA oscillation in Figure 3A	[S9]; This study
SJ_FS116	SJ_FS104 transduction of *kan-yPet-dnaN*	FtsZ oscillation ($5 \leftrightarrow 10\mu M$ IPTG) in Figure 4B	This study
SJ_FS117	VIP205 transduction of *kan-yPet-dnaN*	FtsZ oscillation ($0 \leftrightarrow 10\mu M$ IPTG) in Figure 4B	This study
SJ1725	SJ81 recombineering of ΔftsZ::[*ftsZ55-mVenus-56*]; confirmed by sequencing	FtsZ concentration measurement (steady-state) in Figures 5 and 7A	This study
SJ_FS119	VIP205 recombineering of ΔftsZ::[*ftsZ55-mVenus-56 tetA-sacB*]; confirmed by sequencing	FtsZ concentration measurement (oscillation) in Figure 6	This study
SJ_FS122	SJ_XTL219 *clpX* sgRNA, *clpX*; transduction of *kan-yPet-dnaN*	ClpX repression with replisome tracking in Figure 7A	This study
SJ_FS123	SJ_XTL219 *clpX* sgRNA, *clpX*; recombineering of ΔftsZ::[*ftsZ55-mVenus-56 tetA-sacB*]	ClpX repression with FtsZ concentration measurement in Figure 7B	This study

Table S1: Strain Information of *E. coli*. Related to the STAR Methods.

B. subtilis strains	Genotype	Experiments used	Notes
PAW885	JH642, *dnaN-mgfpmut2-spec*	–	[S10, S11]
SJ_BS29	PAW885 transformation of motAB::Tn917	–	This study
SEV645	SJ_BS29 transformation of ftsZ::cm and thrC::Pxyl-ftsZ	steady state and FtsZ oscillation in Figure 4B	This study

Table S2: Strain Information of *B. subtilis*. Related to the STAR Methods.

Experiment Name	Strain	Media	Perturbation Parameters	Sample size	Position in figures (symbols)
Nutrient limitation (NCM3722)	SJ_FS103	arginine glucose glucose + 12 a.a.	steady state	1,256 1,328 1,230	1D (●) 1A-1D (●) 1D (●)
Nutrient limitation (MG1655)	SJ_FS104	M9 acetate glucose glycerol + 11 a.a.	steady state	1,077 1,640 1,465	7A (●) 1D (●) 1D (●), 2A 3A, 4B (●)
Chloramphenicol	SJ_FS103	glucose	6μM	1,232	1D (●)
Fosfomycin	SJ_FS104	glycerol + 11 a.a.	0.05μg/ml	992	1D (■)
DnaA knockdown	SJ_FS105	glycerol + 11 a.a.	30μM arabinose	704	1D (▼)
DnaA overexpression	SJ_DL91	glucose	0.4mM IPTG	890	1D (▲)
SulA overexpression	SJ_FS110	glucose	60μM IPTG	1,164	1D (♦)
DnaA oscillation (overexpression)	SJ_FS112	glycerol + 11 a.a.	0mM↔1mM IPTG; period = 4 hours	1,070	3A (■)
DnaA oscillation (underexpression)	SJ1436	glucose	0mM↔0.2mM IPTG; period = 4 hours	1,259	3A (●)
FtsZ oscillation	SJ_FS117	glycerol + 11 a.a.	5μM↔10μM IPTG; period = 4 hours	1,258	S4C (●)
			0μM↔10μM IPTG; period = 4 hours	1,673	4B (●)
FtsZ oscillation in *B. subtilis*	SEV645	$S7_{50}$ mannose	steady state 1%(w/v) xylose	606	4B (●)
			oscillation 0.1%↔1%(w/v) xylose; period = 4 hours	608	4B (■)
FtsZ concentration measurement	SJ1725	glycerol + 11 a.a.	steady state	1,433	5 (●)
		M9 acetate		8,492	7B (○)
FtsZ concentration measurement	SJ_FS119	glycerol + 11 a.a.	steady state	842	5 (●)
			oscillation 0μM↔20μM IPTG; period = 4 hours	894	6 (exp1 ●)
				666	6 (exp2 ●)
ClpX repression plus replisome tracking	SJ_FS122	M9 acetate	steady state	1,055	7A (●)
ClpX repression plus FtsZ concentration measurement	SJ_FS123	M9 acetate	steady state	2,341	7B (○)

Table S3: Experimental conditions and sample size. Related to the STAR Methods.
The sample size represents the number of single cell division cycles measured from each mother machine experiment. The symbols in the rightmost columns are the same as those in the corresponding main figures. '↔' indicates that the oscillation experiment was conducted between the two concentrations of inducer on both sides.

SUPPLEMENTAL REFERENCES

[S1] Si, F., Li, D., Cox, S.E., Sauls, J.T., Azizi, O., Sou, C., Schwartz, A.B., Erickstad, M.J., Jun, Y., Li, X., and Jun, S. (2017). Invariance of initiation mass and predictability of cell size in *Escherichia coli*. Curr. Biol. *27*, 1278–1287.

[S2] Lyons, E., Freeling, M., Kustu, S., and Inwood, W. (2011). Using genomic sequencing for classical genetics in *E. coli* K12. PLoS ONE *6*, e16717.

[S3] Brown, S.D., and Jun, S. (2015). Complete genome sequence of *Escherichia coli* NCM3722. Genome Announc. *3*, e00879–15.

[S4] Li, X., Jun, Y., Erickstad, M.J., Brown, S.D., Parks, A., Court, D.L., and Jun, S. (2016). tCRISPRi: tunable and reversible, one-step control of gene expression. Sci. Rep. *6*, 39076.

[S5] Garrido, T., Sánchez, M., Palacios, P., Aldea, M., and Vicente, M. (1993). Transcription of FtsZ oscillates during the cell cycle of *Escherichia coli*. EMBO J. *12*, 3957–65.

[S6] Reyes-Lamothe, R., Sherratt, D.J., and Leake, M.C. (2010). Stoichiometry and architecture of active DNA replication machinery in *Escherichia coli*. Science *328*, 498–501.

[S7] Amir, A., Babaeipour, F., Mcintosh, D.B., Nelson, D.R., and Jun, S. (2014). Bending forces plastically deform growing bacterial cell walls. Proc. Natl. Acad. Sci. U.S.A. *111*, 5778–5783.

[S8] Nishida, S., Fujimitsu, K., Sekimizu, K., Ohmura, T., Ueda, T., and Katayama, T. (2002). A nucleotide switch in the *Escherichia coli* DnaA protein initiates chromosomal replication evidence from a mutant DnaA protein defective in regulatory ATP hydrolysis in vitro and in vivo. J. Biol. Chem. *277*, 14986–14995.

[S9] Riber, L., Olsson, J.A., Jensen, R.B., Skovgaard, O., Dasgupta, S., Marinus, M.G., and Løbner-Olesen, A. (2006). Hda-mediated inactivation of the DnaA protein and DnaA gene autoregulation act in concert to ensure homeostatic maintenance of the *Escherichia coli* chromosome. Genes Dev. *20*, 2121–2134.

[S10] Goranov, A.I., Breier, A.M., Merrikh, H., and Grossman, A.D. (2009). YabA of *Bacillus subtilis* controls DnaA-mediated replication initiation but not the transcriptional response to replication stress. Mol. Microbiol. *74*, 454–466.

[S11] Mangiameli, S.M., Veit, B.T., Merrikh, H., and Wiggins, P.A. (2017). The replisomes remain spatially proximal throughout the cell cycle in bacteria. PLoS Genet. *13*, e1006582.